Multiscale technique for nonlinear analysis of elastoplastic and viscoplastic composites*

Sonia Marfia, Elio Sacco

Dipartimento di Ingegneria Civile e Meccanica, Universitá di Cassino e del Lazio Meridionale, Via G. Di Biasio 43, 03043 Cassino, Italy

Abstract

Aim of the present paper is to develop an efficient multiscale procedure for studying the mechanical response of structural elements made of elastoplastic or viscoplastic composite materials. The micro and the macro scales are considered separated. At the microscale a PieceWise Uniform Transformation Field Analysis (PWUTFA) homogenization technique is adopted to derive the overall response of a periodic composite. Thus, a Unit Cell (UC) containing all the properties of the heterogeneous material is analyzed and divided in subsets; in each one the inelastic strain is considered uniform, i.e. constant, and represents the history variable of the analysis. Elastoplastic and elasto-viscoplastic models with isotropic hardening are adopted in order to describe the nonlinear response of the constituents. A new numerical procedure is developed in order to solve the evolutive problem in all the subsets simultaneously adopting a predictor-corrector technique. The corrector phase is solved by means of a modified Newton-Raphson iterative procedure. Furthermore, the tangent consistent with the algorithm is computed and adopted in the multiscale computations. Numerical applications are carried out in order to assess the efficiency of the proposed multiscale approach.

Keywords: Composites, Multiscale analysis, Homogenization, TFA, Plasticity, Viscoplasticity.

*In press on Composites Part B: Engineering, https://doi.org/10.1016/j.compositesb.2017.10.015

1 Introduction

Composite materials often present internally complex microstructures, therefore, they require specific formulations to be developed in order to take into account the mechanical behavior of each component and its topological distribution. In particular, if the constituents are characterized by a nonlinear response the study becomes more complex as the nonlinear effect occurring in the material should also be modeled. Lately, the interest around the modeling of composite materials has increased significantly.

A large class of composite media are made of constituents that exhibit plastic and time-dependent behavior that requires the use of nonlinear elastoplastic and elasto-viscoplastic material models. Recently, innovative composite characterized by plastic and viscoplastic response of the constituents have been presented, among the other, in [42, 2, 13, 27].

One possibility to evaluate the overall mechanical response of these composite materials, which have complex microstructures and viscoplastic effects in its constituents, is to adopt micromechanical procedures, that study a representative volume element (RVE), determining the behavior of the homogenized equivalent material. Very recently, micromechanical numerical investigation have been presented, for example, in 2D plasticity [26] or in 3D viscoplasticity [7, 39] framework for composites materials.

In order to perform analyses of structural elements, made of composite materials, a multiscale approach can be adopted considering the complex nonlinear response of these composites directly derived from a micromechanical analysis. The multiscale technique consists in the modeling of the structure taking into account two different scales: the macro-scale, i.e. the scale at the structural level, and the micro-scale, i.e. the scale at the material level, where the single heterogeneity can be distinguished in the material. If the heterogeneity size is significantly smaller than the structural size, the two scales can be considered separated and it is possible to solve the micromechanical problem at each point of the structure and to adopt the obtained results for deriving the constitutive response to be used for the structural analysis.

A major problem in the multiscale analysis is the development of an effective, i.e. simple and accurate, solution of the micromechanical problem. In fact, the multiscale problem can be solved using nonlinear finite element (FE) analyses both at the material and at the structural level, i.e. the FE^2 multiscale scheme [17]. The FE^2 is developed inducing a large number of history variables that can lead to very high computational burden and time. In order to improve the multiscale approach and to reduce the number of history variables, the nonlinear overall response of the composite can be derived adopting simplified homogenization tech-

niques. In literature, several techniques have been presented for solving the homogenization problem of plastic and viscoplastic composites. Among the others, recently, Caporale et al. [4, 3] proposed a technique based on eigenstrain and Fourier series for the homogenization of elastic and viscoelastic periodic composites. Czarnota et al. [11] proposed a homogenization approach based on an additive tangent Mori–Tanaka scheme in order to study two-phase composites with spherical inclusion and nonlinear elasto–viscoplastic behavior. Mareau and Berbenni [28] presented a homogenization technique based on the self-consistent approximation for heterogeneous viscoplastic materials. Agoras et al. [1] presented a homogenization technique modeling the nonlinearity and the heterogeneity of the properties in the phases with the variational procedure proposed in [37].

An efficient homogenization approach for nonlinear material is the Transformation Field Analysis (TFA), originally proposed by Dvorak [14], that determines the behavior of the composite taking into account the nonlinear phenomena considering the presence of inelastic strain fields. Lately, the TFA approach has been adopted to derive the response of several nonlinear composites considering a uniform [30], piecewise uniform [15, 6, 40] or nonuniform [33, 18, 19, 38, 20, 41, 23, 32, 9, 10, 24] distribution of the inelastic strain. The proposed TFA approaches differ mainly for the approximation adopted for the inelastic strain and for the procedure used to evaluate the evolution of the history variables [25]. Some of these approaches, in particular the ones based on the nonuniform TFA, are very accurate but, at the same time, they could become computationally expensive.

Some multiscale analyses have been performed developing the TFA homogenization technique at the microlevel. Michel and Suquet [34] proposed a multiscale approach for studying structural elements made of viscoplastic composites and considering at the microlevel the TFA procedure proposed in [33]; they compared the response of the homogenized structure with the response of the actual heterogeneous structure computed with a very fine discretization. Marfia and Sacco [31] studied the behavior of SMA composite laminates adopting at the material level the TFA technique presented in [29]. Fritzen et al. [22, 21] developed a multiscale approach considering at the microlevel the TFA technique proposed in [23] to derive the mechanical behavior of viscoplastic composites. Zhang and Oskay [43] proposed a multiscale approach extending the eigenstrain-based reduced order modeling approach to solve problems characterized by non separable scales.

A high computational efficiency is required for these multiscale approaches in order to be able to perform structural analyses of composite materials without having too long time of computation and too high number of history variables. For this reason, a compromise between accuracy and computational effort should be fulfilled. Hence, the research is very

active in this field, aimed at developing efficient multiscale algorithms.

Starting from these considerations, the present paper has the scope of proposing a new and efficient multiscale procedure for studying the response of structural elements made of composite materials whose constituents present plastic or viscoplastic behavior. In particular, periodic composite are studied, thus a repetitive Unit Cell (UC) containing all the properties of the heterogeneous material is analyzed by means of a PieceWise Uniform TFA (PWUTFA) homogenization technique. This choice is made with the aim to obtain a satisfactorily accurate homogenization technique, resulting particularly efficient from the computational point of view for the multiscale analysis. The UC is divided in subsets and in each one the inelastic strain is considered uniform, i.e. constant. Elastoplastic and elasto-viscoplastic models with isotropic hardening are introduced in order to describe the nonlinear response of the constituents.

A new numerical procedure is proposed solving the evolutive problem in all the subsets simultaneously, adopting a predictor-corrector technique. The corrector phase is solved by means of a modified Newton-Raphson iterative procedure. In order to obtain an efficient numerical tool, the tangent consistent with the algorithm is evaluated and adopted in the computations.

Numerical applications are developed in order to assess the efficiency of the proposed multiscale approach. In particular, the proposed procedure is implemented in a two-dimensional framework, considering the plane stress condition. The homogenization is performed at the Gauss point level of the 3 node optimum membrane triangular (OPT) element proposed in [16] and recently extended to corotational and material nonlinear behavior in [5, 35]. A comparison between the proposed multiscale technique and a micromechanical structural analysis is carried out.

The remaining part of the paper is organized as follows. In Section 2, the multiscale approach is described; in Section 3, the PWUTFA homogenization technique is illustrated; in Section 4, the numerical procedure is presented; in Section 5, the numerical applications are reported and, finally, Section 6 contains some concluding remarks.

In the following the Voigt notation is adopted, so that second-order tensors are represented as vectors, while fourth-order tensors as matrices.

2 Multiscale approach

2.1 Macroscale

A heterogeneous body $\mathcal{B}$, subjected to volume forces $\mathbf{b}$ is considered. The boundary $\partial\mathcal{B}$ is split in two parts $\partial_u\mathcal{B}$, where the displacement conditions $\hat{\mathbf{U}}$ are prescribed, and $\partial_f\mathcal{B}$, where the surface forces $\mathbf{p}$ are applied, with $\partial B = \partial_u\mathcal{B} \cup \partial_f\mathcal{B}$ and $\partial_u\mathcal{B} \cap \partial_f\mathcal{B} = \emptyset$. The global Cartesian coordinate system (X_1, X_2, X_3) is introduced at the macroscale. The displacement field is denoted by the vector $\mathbf{U}(\mathbf{X}) = \{U_1\, U_2\, U_2\}^T$ with $\boldsymbol{X} = \{X_1\, X_2\, X_3\}^T$ the position vector of a typical point of $\mathcal{B}$. The strain field $\mathbf{E} = \{E_{11}\, E_{22}\, E_{33}\, \Gamma_{12}\, \Gamma_{23}\, \Gamma_{13}\}^T$ is obtained as:

$$
\begin{aligned}
E_{11} &= \frac{\partial U_1}{\partial X_1} \\
E_{22} &= \frac{\partial U_2}{\partial X_2} \\
E_{33} &= \frac{\partial U_3}{\partial X_3} \\
\Gamma_{12} &= \frac{\partial U_1}{\partial X_2} + \frac{\partial U_2}{\partial X_1} \\
\Gamma_{23} &= \frac{\partial U_2}{\partial X_3} + \frac{\partial U_3}{\partial X_2} \\
\Gamma_{13} &= \frac{\partial U_1}{\partial X_3} + \frac{\partial U_3}{\partial X_1}
\end{aligned}
\qquad . \tag{1}
$$

The stress field, denoted by $\boldsymbol{\Sigma} = \{\Sigma_{11}\, \Sigma_{22}\, \Sigma_{33}\, \Sigma_{12}\, \Sigma_{23}\, \Sigma_{13}\}^T$, has to satisfy the classical equilibrium equations.

It is assumed that the body is made of a composite material, whose microstructural size is significantly smaller than the characteristic dimension of the body; thus, the macro and microscale can be considered separated. In this case, the constitutive equations of the macroscale can be recovered by performing a homogenization of the composite at the micro level as described in the following. For this reason, the constitutive equations are not specified at this level.

2.2 Microscale

A periodic microstructure is assumed for the composite material. Because of the periodicity, a unit cell (UC) can be considered for studying the response of the composite. In particular, the UC is chosen as a parallelepipedal solid, defining the heterogeneous body Ω containing

all the geometrical and material information of the composite. Introducing a local coordinate reference system (x_1, x_2, x_3) at the microscale, the UC has dimensions $2\,a_1 \times 2\,a_2 \times 2\,a_3$ and volume V.

2.2.1 Kinematics

The kinematics of the UC is characterized by the following representation form of the displacement field:

$$\mathbf{u}\,(\mathbf{x}) = \mathbf{A}\,\mathbf{E} + \mathbf{u}^*\,(\mathbf{x})\ , \tag{2}$$

where:

- $\mathbf{E}$ is the macroscopic deformation, introduced above by equations (1), evaluated at the material point of the equivalent macroscopic medium linked to the considered UC, and it is considered as the overall strain, i.e. the average strain in the UC;
- $\mathbf{A}$ is the matrix defining the kinematical map, given by:

$$\mathbf{A} = \begin{bmatrix} x_1 & 0 & 0 & \frac{1}{2}x_2 & 0 & \frac{1}{2}x_3 \\ 0 & x_2 & 0 & \frac{1}{2}x_1 & \frac{1}{2}x_3 & 0 \\ 0 & 0 & x_3 & 0 & \frac{1}{2}x_2 & \frac{1}{2}x_1 \end{bmatrix}\ ; \tag{3}$$

- $\mathbf{u}^*\,(\mathbf{x})$ is the periodic part of the displacement field, satisfying the periodicity conditions:

$$\begin{array}{rcl} \mathbf{u}^*\,(-a_1,\ \ x_2,\ \ x_3) & = & \mathbf{u}^*\,(a_1, x_2, x_3) \\ \mathbf{u}^*\,(\ \ x_1, -a_2,\ \ x_3) & = & \mathbf{u}^*\,(x_1, a_2, x_3)\ . \\ \mathbf{u}^*\,(\ \ x_1,\ \ x_2, -a_3) & = & \mathbf{u}^*\,(x_1, x_2, a_3) \end{array} \tag{4}$$

Taking into account equations (2) and (3), the strain field in the UC, $\boldsymbol{\varepsilon} = \{\varepsilon_{11}\ \varepsilon_{22}\ \varepsilon_{33}\ \gamma_{12}\ \gamma_{23}\ \gamma_{13}\}^T$, is obtained as:

$$\boldsymbol{\varepsilon}\,(\mathbf{x}) = \mathbf{E} + \boldsymbol{\varepsilon}^*\,(\mathbf{x}) \qquad \text{with} \quad \begin{array}{rcl} \varepsilon^*_{11} & = & u^*_{1,1} \\ \varepsilon^*_{22} & = & u^*_{2,2} \\ \varepsilon^*_{33} & = & u^*_{3,3} \\ \gamma^*_{12} & = & u^*_{1,2} + u^*_{2,1} \\ \gamma^*_{23} & = & u^*_{2,3} + u^*_{3,2} \\ \gamma^*_{13} & = & u^*_{1,3} + u^*_{3,1} \end{array}\ , \tag{5}$$

where the pedex $,i$ indicates the partial derivative with respect to x_i. As the periodic part of the displacement $\mathbf{u}^*(\mathbf{x})$ satisfies the boundary conditions (4), the average of the strain field $\boldsymbol{\varepsilon}^*(\mathbf{x})$ is null, so that the average of the strain field in the UC is equal to $\mathbf{E}$.

2.2.2 Plasticity and viscoplasticity constitutive models

It is assumed that the materials which constitute the composite exhibit a plastic or viscoplastic behavior. Plasticity models take into account the inelastic strains while viscoplasticity models are able to account for both rheologic and plastic effects occurring in the material. It is assumed that the strain can be divided into an elastic and inelastic part due only to plastic effects for the plasticity model and to viscous and plastic effects for the viscoplastic model. In both cases, the constitutive law is written as:

$$\boldsymbol{\sigma} = \mathbf{C}\left(\boldsymbol{\varepsilon} - \boldsymbol{\pi}\right), \tag{6}$$

where $\boldsymbol{\sigma} = \{\sigma_{11}\,\sigma_{22}\,\sigma_{33}\,\tau_{12}\,\tau_{23}\,\tau_{13}\}^T$ represents the stress vector at the point $\mathbf{x}$, $\mathbf{C}$ is the 6×6 matrix containing the material elasticities and $\boldsymbol{\pi}$ is the inelastic strain due to the plastic or viscous response.

The viscoplasticity problem is both time and loading history dependent, thus, the stress and strain fields are time dependent and the plastic properties are loading path dependent. According to Perzyna [36], elasto-viscoplastic materials show viscous properties in the plastic region; thus, a dissipation potential is introduced and the assumption of the existence of an elastic domain, where there are no viscous effects, is considered. Two constitutive models, one based on plasticity (P) and the other one on viscoplasticity (VP) are presented in this Section. Since the material does not show viscous properties in the elastic region, the classical Mises yield function is considered in the framework of associated plasticity [12], with isotropic hardening; thus, for both the models the limit function is introduced:

$$f = q - \sigma_y - H\kappa \qquad \text{with } q = \sqrt{\frac{3}{2}\,\boldsymbol{\sigma}^T\mathbf{M}\,\boldsymbol{\sigma}}\,, \tag{7}$$

where H is the isotropic hardening parameter, κ is the accumulated plastic strain:

$$\kappa = \int_0^t \|\dot{\boldsymbol{\pi}}\|\,dt\,, \tag{8}$$

and $\mathbf{M}$ is the matrix defined as:

$$\mathbf{M} = \frac{1}{3}\begin{bmatrix} 2 & -1 & -1 & 0 & 0 & 0 \\ -1 & 2 & -1 & 0 & 0 & 0 \\ -1 & -1 & 2 & 0 & 0 & 0 \\ 0 & 0 & 0 & 6 & 0 & 0 \\ 0 & 0 & 0 & 0 & 6 & 0 \\ 0 & 0 & 0 & 0 & 0 & 6 \end{bmatrix}. \tag{9}$$

The evolutive associate laws result:

$$\begin{aligned} \dot{\boldsymbol{\pi}} &= \dot{\lambda}\frac{\partial f}{\partial \boldsymbol{\sigma}} = \dot{\lambda}\mathbf{N}(\boldsymbol{\sigma}) \\ \dot{\kappa} &= \dot{\lambda} \end{aligned} \tag{10}$$

where $\dot{\lambda}$ is the plastic multiplier and $\mathbf{N}(\boldsymbol{\sigma})$ is the normal vector resulting:

$$\mathbf{N}(\boldsymbol{\sigma}) = \frac{3}{2\,q}\,\mathbf{M}\,\boldsymbol{\sigma}\,. \tag{11}$$

For the plasticity model the multiplier $\dot{\lambda}$ is evaluated considering the Kuhn-Tucker and the consistency conditions:

$$\dot{\lambda} \geq 0 \qquad f \leq 0 \qquad \dot{\lambda} f = 0 \qquad\qquad \dot{\lambda}\dot{f} = 0\,. \tag{12}$$

For the viscoplastic model (VP) proposed by Perzyna [36], the plastic multiplier results:

$$\dot{\lambda} = \begin{cases} \dfrac{1}{\mu}\left[\dfrac{q}{\sigma_y - H\kappa} - 1\right]^{1/\epsilon} & \text{if } f(\boldsymbol{\sigma}) \geq 0 \\ 0 & \text{if } f(\boldsymbol{\sigma}) < 0 \end{cases}, \tag{13}$$

where μ is a viscosity-related parameter and ϵ is the non-dimensional rate sensitivity parameter $\epsilon \in (0, 1)$. Both parameters are strictly positive and temperature dependent. The set of history variables for the plastic and viscoplastic material is denoted by $\boldsymbol{\chi} = (\boldsymbol{\pi}, \kappa)$.

3 PWUTFA homogenization technique

Assigned the macroscopic strain $\mathbf{E}$ in the UC, the micromechanical problem consists in:

- finding
  - the displacement field $\mathbf{u}(\mathbf{x})$,
  - the total strain field $\boldsymbol{\varepsilon}(\mathbf{x})$,
  - the set of internal variables $\boldsymbol{\chi}$,
  - the stress field $\boldsymbol{\sigma}(\mathbf{x})$,
- which satisfy the classical governing equations of the Continuum Mechanics, i.e. compatibility, equilibrium and constitutive relationships with suitable boundary conditions.

The micromechanical problem can be solved making use of a suitable numerical procedure. In particular, the finite element method is classically adopted to derive the micromechanical response of the UC. Once the micromechanical problem is solved, the overall response of the UC is determined; in particular, the average stress, representing the stress at the macroscopic level, can be computed as:

$$\boldsymbol{\Sigma} = \frac{1}{V}\int_{\Omega} \boldsymbol{\sigma}\, dV\,, \tag{14}$$

when no voids or fracture are present in the UC.

Because of the complexity and of the computational cost of the micromechanical nonlinear finite element approach, simplified and approximated techniques can be developed. In particular, the TFA (Transformation Field Analysis) technique is herein adopted [14, 41].

The UC is split in n homogeneous subsets, with the $s-$th subset Ω_s characterized by a volume V_s. The subsets satisfy the relationships $\bigcup_{s=1}^{n}\Omega_s = \Omega$ and $\bigcap_{s=1}^{n}\Omega_s = \emptyset$. The TFA procedure can be regarded as an application of the coaction theory [8] and it can be performed according to the steps reported in the following.

1. The constitutive equation (6) is written in the $s-$th subset Ω^s:

$$\boldsymbol{\sigma}^s = \mathbf{C}^s\left(\boldsymbol{\varepsilon}^s - \boldsymbol{\pi}^s\right)\,, \tag{15}$$

   where $\mathbf{C}^s$ is the matrix of the elasticities of the material of subset Ω^s and $\boldsymbol{\pi}^s$ is assumed to be constant (uniform) in Ω^s.

2. The uniform inelastic strain $\boldsymbol{\pi}^s$ is considered as a coaction, i.e. an eigenstrain, in the subset Ω^s.

3. The effects of the prescribed macroscopic deformation $\mathbf{E}$ arising in each subset Ω^j $(j = 1, .., n)$ is determined through the introduction of n localization 6×6 matrices

$\mathbf{L}_E^j(\mathbf{x})$ able to evaluate the local strain and, hence, the local stress at $\mathbf{x} \in \Omega^j$ due to $\mathbf{E}$ by the relationships:

$$\begin{aligned} \mathbf{e}^j(\mathbf{x}) &= \mathbf{L}_E^j(\mathbf{x})\,\mathbf{E}\,, \\ \boldsymbol{\sigma}_e^j(\mathbf{x}) &= \mathbf{C}^j\mathbf{e}^j(\mathbf{x}) \end{aligned} \tag{16}$$

4. The effects of the uniform inelastic strain $\boldsymbol{\pi}^s$ arising in each subset Ω^j $(j = 1, .., n)$ is determined introducing the n^2 localization matrices $\mathbf{L}_{\pi^s}^j(\mathbf{x})$, with dimensions 6×6, able to give the local total $\mathbf{p}^{js}$ and elastic $\boldsymbol{\eta}^{js}$ strain and the local stress $\boldsymbol{\sigma}_{\pi^s}^j$ at $\mathbf{x} \in \Omega^j$ due to $\boldsymbol{\pi}^s$ as:

$$\begin{aligned} \mathbf{p}^{js}(\mathbf{x}) &= \mathbf{L}_{\pi^s}^j(\mathbf{x})\,\boldsymbol{\pi}^s \\ \boldsymbol{\eta}^{js}(\mathbf{x}) &= \mathbf{p}^{js}(\mathbf{x}) - \delta_{js}\boldsymbol{\pi}^s\,, \\ \boldsymbol{\sigma}_{\pi^s}^j(\mathbf{x}) &= \mathbf{C}^j\boldsymbol{\eta}^{js}(\mathbf{x}) \end{aligned} \tag{17}$$

where δ_{js} is the Kroneker index ($\delta_{js} = 1$ if $j \neq s$, $\delta_{js} = 0$ otherwise)

5. The set of all the inelastic strains defined in the subsets Ω^s $(s = 1, .., n)$ are arranged in a unique vector $\boldsymbol{\Pi} = \{\boldsymbol{\pi}^1\ \boldsymbol{\pi}^2\ ...\ \boldsymbol{\pi}^n\}^T$, so that the local total $\mathbf{p}^j$ and elastic $\boldsymbol{\eta}^j$ strain and the local stress $\boldsymbol{\sigma}_\Pi^j$ at $\mathbf{x} \in \Omega^j$ due to $\boldsymbol{\Pi}$ results:

$$\begin{aligned} &\mathbf{p}^j(\mathbf{x}) = \mathbf{L}_\Pi^j(\mathbf{x})\,\boldsymbol{\Pi}\,. \\ &\boldsymbol{\eta}^j(\mathbf{x}) = \mathbf{p}^j(\mathbf{x}) - \boldsymbol{\Delta}^j\,\boldsymbol{\Pi} \\ &\boldsymbol{\sigma}_\Pi^j(\mathbf{x}) = \mathbf{C}^j\boldsymbol{\eta}^j(\mathbf{x}) \end{aligned} \tag{18}$$

where the $6 \times 6n$ localization matrix $\mathbf{L}_\Pi^j(\mathbf{x})$ is obtained assembling the n matrices $\mathbf{L}_{\pi^s}^j(\mathbf{x})$ $(s = 1, .., n)$ and $\boldsymbol{\Delta}^j$ is $6 \times 6\,n$ matrix whose components are $\Delta_{hm}^j = \delta_{hk}$ with $m = 6\,(j-1) + k$.

6. The solution is determined superimposing the effects of the prescribed macroscopic deformation $\mathbf{E}$ with the ones due to inelastic strains arranged in $\boldsymbol{\Pi}$. In particular, the total strain in the subset Ω^j is obtained as the sum of the contributions given by equations (16) and (18):

$$\boldsymbol{\varepsilon}^j(\mathbf{x}) = \mathbf{e}^j(\mathbf{x}) + \mathbf{p}^j(\mathbf{x}) = \mathbf{L}_E^j(\mathbf{x})\,\mathbf{E} + \mathbf{L}_\Pi^j(\mathbf{x})\,\boldsymbol{\Pi}\,. \tag{19}$$

In order to evaluate the inelastic strain, it is necessary to compute the average strain in

each subset of the UC; taking into account equations (16) and (18), the average strains in the typical subset Ω^j due to the prescribed macroscopic deformations $\mathbf{E}$ and to the inelastic strain $\mathbf{\Pi}$ are obtained as as:

$$\overline{\mathbf{e}}^j = \overline{\mathbf{L}}_E^j \, \mathbf{E} \tag{20}$$

$$\overline{\mathbf{p}}^j = \overline{\mathbf{L}}_\Pi^j \, \mathbf{\Pi} \, , \tag{21}$$

where the average in each subset of the localization matrices $\mathbf{L}_e^j(\mathbf{x})$ and $\mathbf{L}_{\mathbf{\Pi}}^j(\mathbf{x})$ are computed as:

$$\overline{\mathbf{L}}_E^j = \frac{1}{V_j} \int_{\Omega^j} \mathbf{L}_E^j(\mathbf{x}) \; dV \qquad \overline{\mathbf{L}}_\Pi^j = \frac{1}{V_j} \int_{\Omega^j} \mathbf{L}_{\mathbf{\Pi}}^j(\mathbf{x}) \; dV \, . \tag{22}$$

Thus, the average total strain $\overline{\boldsymbol{\varepsilon}}^j$ in the $j-$th subset is evaluated as:

$$\overline{\boldsymbol{\varepsilon}}^j = \overline{\mathbf{e}}^j + \overline{\mathbf{p}}^j = \overline{\mathbf{L}}_E^j \, \mathbf{E} + \overline{\mathbf{L}}_\Pi^j \mathbf{\Pi} \, . \tag{23}$$

The procedure for the determination of the micromechanical response of the UC consists in the following steps. Initially, $6 + 6\,n$ micromechanical problems of the UC have to be solved:

- 6 problems corresponding to the UC subjected to the prescribed unit value of only one component of the macroscopic deformation $\mathbf{E}$; in such a way, it is possible to evaluate the 6 columns of the localization matrix $\overline{\mathbf{L}}_E^j$ for all the subsets Ω^j $(j = 1, .., n)$;
- $6\,n$ problems prescribing a unit value of only one component of the inelastic strains collected in the vector $\mathbf{\Pi}$ under the condition of null average strain in the UC; this allows to determine the $6\,n$ columns of the localization matrix $\overline{\mathbf{L}}_\Pi^j$ for all the subsets Ω^j $(j = 1, .., n)$.

Accounting for equations $(18)_1$, $(18)_2$ and (21), the average elastic strain $\overline{\boldsymbol{\eta}}^j$ in the $j-$th subset due to the eigenstrain $\mathbf{\Pi}$ is obtained as:

$$\overline{\boldsymbol{\eta}}^j = \overline{\mathbf{p}}^j - \boldsymbol{\pi}^j = \left(\overline{\mathbf{L}}_\Pi^j - \boldsymbol{\Delta}^j \right) \mathbf{\Pi} \, . \tag{24}$$

Once the localization rectangular matrices $\overline{\mathbf{L}}_E^j$ (with $j = 1, .., n$) are determined, using the Hill-Mandel equation, the overall macroscopic stress $\mathbf{\Sigma}_E$ due to the macroscopic deformation

$\mathbf{E}$ is evaluated as:

$$\begin{aligned} \delta\mathbf{E}^T\boldsymbol{\Sigma}_E &= \frac{1}{V}\int_V \delta\mathbf{e}^T\boldsymbol{\sigma}_e\, dV \\ &= \frac{1}{V}\sum_{j=1}^{n}\left(\delta\overline{\mathbf{e}}^j\right)^T\mathbf{C}^j\overline{\mathbf{e}}^j V^j\,, \end{aligned} \tag{25}$$

where $\mathbf{C}^j$ is the elastic matrix of the subset Ω^j. Setting $\rho_j = V_j/V$ and taking into account equation (20), it results:

$$\delta\mathbf{E}^T\boldsymbol{\Sigma}_E = \sum_{j=1}^{n}\rho_j\left(\overline{\mathbf{L}}_E^j\,\delta\mathbf{E}\right)^T\mathbf{C}^j\overline{\mathbf{L}}_E^j\,\mathbf{E}\,, \tag{26}$$

which gives:

$$\boldsymbol{\Sigma}_E = \overline{\mathbf{C}}\,\mathbf{E} \tag{27}$$

$\overline{\mathbf{C}}$ being the overall elastic matrix of the UC obtained as:

$$\overline{\mathbf{C}} = \sum_{j=1}^{n}\rho_j\left(\overline{\mathbf{L}}_E^j\right)^T\mathbf{C}^j\overline{\mathbf{L}}_E^j\,. \tag{28}$$

Analogously, the overall macroscopic stress $\boldsymbol{\Sigma}_{\boldsymbol{\Pi}}$ in the whole UC due to the presence of $\boldsymbol{\Pi}$ is computed as:

$$\begin{aligned} \delta\mathbf{E}^T\boldsymbol{\Sigma}_\Pi &= \frac{1}{V}\int_V \delta\mathbf{e}^T\boldsymbol{\sigma}_\Pi\, dV \\ &= \sum_{j=1}^{n}\rho_j\left(\overline{\mathbf{L}}_E^j\,\delta\mathbf{E}\right)^T\mathbf{C}^j\left(\overline{\mathbf{L}}_\Pi^j - \boldsymbol{\Delta}^j\right)\boldsymbol{\Pi}\,, \end{aligned} \tag{29}$$

which gives:

$$\boldsymbol{\Sigma}_\Pi = \sum_{j=1}^{n}\rho_j\left(\overline{\mathbf{L}}_E^j\right)^T\mathbf{C}^j\left(\overline{\mathbf{L}}_\Pi^j - \boldsymbol{\Delta}^j\right)\boldsymbol{\Pi}\,. \tag{30}$$

Finally, the overall macroscopic deformation in the UC is equal to $\mathbf{E}$, while the overall macroscopic stress is equal to the sum of $\boldsymbol{\Sigma}_E$ and $\boldsymbol{\Sigma}_\Pi$, given by equations (27) and (30), respectively, leading to:

$$\boldsymbol{\Sigma} = \overline{\mathbf{C}}\,\mathbf{E} + \sum_{j=1}^{n}\rho_j\left(\overline{\mathbf{L}}_E^j\right)^T\mathbf{C}^j\left(\overline{\mathbf{L}}_\Pi^j - \boldsymbol{\Delta}^j\right)\boldsymbol{\Pi}\,, \tag{31}$$

where formula (30) is taken into account.

The average plastic strain $\overline{\mathbf{p}}$ is defined from equation (31) as:

$$\overline{\mathbf{p}} = \overline{\mathbf{C}}^{-1} \left[\sum_{j=1}^{n} \rho_j \left(\overline{\mathbf{L}}_E^j \right)^T \mathbf{C}^j \left(\overline{\mathbf{L}}_{\mathbf{\Pi}}^j - \boldsymbol{\Delta}^j \right) \mathbf{\Pi} \right] . \tag{32}$$

In the following plastic and viscoplastic constitutive models are introduced to detail completely the procedure.

4 Numerical procedure

At the typical Gauss point of the structural finite element discretization, the homogenization procedure is implemented. In the following, the numerical procedure is described in detail for the case of plastic and viscoplastic material constitutive laws.

4.1 Time step solution

In order to perform the time integration of the evolutive equations (10), a backward Euler technique is used. Once the solution at the time t_n is known, the solution at time t is computed by solving a finite time step. In the following the quantities at time t_n are denoted with the index $_n$ while the quantities at the actual time t are denoted with no index. The finite step is solved adopting a predictor corrector procedure. The history variables of the problem are the uniform inelastic strain $\mathbf{\Pi}$ and the vector $\boldsymbol{\kappa}$ containing the accumulated inelastic strain κ^s in each subset. Note that the material properties of the constituents of the composites can vary from subset to subset but they are assumed uniform in each subset.

A trial state is defined in each subset considering the history variables frozen and equal to the one at the previous step:

$$\begin{aligned}
\mathbf{\Pi} &= \mathbf{\Pi}_n \\
\boldsymbol{\kappa} &= \boldsymbol{\kappa}_n \\
\overline{\boldsymbol{\varepsilon}}^s &= \overline{\mathbf{L}}_E^s \, \mathbf{E} + \overline{\mathbf{L}}_{\Pi}^s \mathbf{\Pi} \\
\boldsymbol{\sigma}^{s,TR} &= \mathbf{C}^s \left(\overline{\boldsymbol{\varepsilon}}^s - \boldsymbol{\pi}^s \right) \\
q^{s,TR} &= \sqrt{\frac{3}{2} \left(\boldsymbol{\sigma}^{s,TR} \right)^T \mathbf{M} \, \boldsymbol{\sigma}^{s,TR}} \\
f^{s,TR} &= q^{s,TR} - \sigma_y^s - H^s \kappa^s
\end{aligned} \quad . \tag{33}$$

If $f^{s,TR} < 0$ in all the subsets the step is elastic and the trial state given by equation (33) is the solution. If $f^{s,TR} \geq 0$ at least in one subset, the correction phase, concerning all the subsets has to be performed. The equations governing the time step are written in the residual form for each subset Ω^s:

$$\begin{array}{rcll} \mathbf{R}^s_{\Delta\pi} & = & \Delta\boldsymbol{\pi}^s - \Delta\lambda^s \dfrac{\partial f^s}{\partial \boldsymbol{\sigma}^s} & = \mathbf{0} \\ \mathbf{R}^s_{\varepsilon} & = & \overline{\boldsymbol{\varepsilon}}^s - \overline{\mathbf{L}}^s_E \, \mathbf{E} - \overline{\mathbf{L}}^s_{\Pi} \boldsymbol{\Pi} & = \mathbf{0} \\ R^s_g & = & g^s & = 0 \end{array} \quad , \tag{34}$$

where the first of (34) is obtained from equation (10); the second of (34) is the residual form of equation (23) and in the third of (34) the quantity g^s is defined as:

$$\begin{array}{rcll} g^s & = & \Delta\lambda^s & \text{if} \quad f^{s,TR} < 0 \\ g^s & = & q^s - \sigma_y - H\kappa^s & \text{if} \quad f^{s,TR} \geq 0 \quad \text{Plasticity} \\ g^s & = & \triangle\lambda^s - \frac{1}{\mu}\left(\frac{q^s}{\sigma_y - H\kappa^s} - 1\right)^{1/\epsilon} & \text{if} \quad f^{s,TR} \geq 0 \quad \text{Viscoplasticity} \end{array} \quad . \tag{35}$$

Writing the system of equation (34) for the all the n subsets, it results:

$$\begin{array}{rcl} \mathbf{R}_{\pi} & = & \Delta\boldsymbol{\Pi} - \left\{ \begin{array}{c} \Delta\lambda^1 \dfrac{\partial f^1}{\partial \boldsymbol{\sigma}^1} \\ \Delta\lambda^2 \dfrac{\partial f^2}{\partial \boldsymbol{\sigma}^2} \\ \ldots \\ \Delta\lambda^n \dfrac{\partial f^n}{\partial \boldsymbol{\sigma}^n} \end{array} \right\} \\ \mathbf{R}_{\varepsilon} & = & \left\{ \begin{array}{c} \overline{\boldsymbol{\varepsilon}}^1 \\ \overline{\boldsymbol{\varepsilon}}^2 \\ \ldots \\ \overline{\boldsymbol{\varepsilon}}^n \end{array} \right\} - \left[\begin{array}{c} \overline{\mathbf{L}}^1_E \\ \overline{\mathbf{L}}^2_E \\ \ldots \\ \overline{\mathbf{L}}^n_E \end{array} \right] \mathbf{E} - \left[\begin{array}{c} \overline{\mathbf{L}}^1_{\Pi} \\ \overline{\mathbf{L}}^2_{\Pi} \\ \ldots \\ \overline{\mathbf{L}}^n_{\Pi} \end{array} \right] (\Delta\boldsymbol{\Pi} + \boldsymbol{\Pi}_n) \, . \\ \mathbf{R}_g & = & \left\{ \begin{array}{c} g^1 \\ g^2 \\ \ldots \\ g^n \end{array} \right\} \end{array} \tag{36}$$

Equations (36) represent a system of $6n + 6n + n$ nonlinear equations in the set of unknowns $\{\Delta\boldsymbol{\Pi}, \boldsymbol{\Gamma}, \boldsymbol{\Lambda}\}$, where $\boldsymbol{\Gamma} = \left\{ \begin{array}{cccc} \overline{\boldsymbol{\varepsilon}}^1 & \overline{\boldsymbol{\varepsilon}}^2 & \ldots & \overline{\boldsymbol{\varepsilon}}^n \end{array} \right\}^T$ and $\boldsymbol{\Lambda} = \left\{ \begin{array}{cccc} \Delta\lambda^1 & \Delta\lambda^2 & \ldots & \Delta\lambda^n \end{array} \right\}^T$. In order to solve the algebraic system of nonlinear equations the modified Newton-Raphson algorithm is adopted; at the typical $p+1-$th iteration, the following linearized problem has to be

solved:

$$\left\{\begin{array}{c}\mathbf{0}\\ \mathbf{0}\\ \mathbf{0}\end{array}\right\} = \left\{\begin{array}{c}\mathbf{R}_\pi\\ \mathbf{R}_\varepsilon\\ \mathbf{R}_g\end{array}\right\}_p + \left[\begin{array}{ccc}\dfrac{\partial \mathbf{R}_\pi}{\partial \mathbf{\Pi}} & \dfrac{\partial \mathbf{R}_\pi}{\partial \mathbf{\Gamma}} & \dfrac{\partial \mathbf{R}_\pi}{\partial \mathbf{\Lambda}}\\ \dfrac{\partial \mathbf{R}_\varepsilon}{\partial \mathbf{\Pi}} & \dfrac{\partial \mathbf{R}_\varepsilon}{\partial \mathbf{\Gamma}} & \dfrac{\partial \mathbf{R}_\varepsilon}{\partial \mathbf{\Lambda}}\\ \dfrac{\partial \mathbf{R}_g}{\partial \mathbf{\Pi}} & \dfrac{\partial \mathbf{R}_g}{\partial \mathbf{\Gamma}} & \dfrac{\partial \mathbf{R}_g}{\partial \mathbf{\Lambda}}\end{array}\right]_p \left\{\begin{array}{c}d\mathbf{\Pi}\\ d\mathbf{\Gamma}\\ d\mathbf{\Lambda}\end{array}\right\}, \tag{37}$$

where the derivatives are explicitly reported in the Appendix.

The variation of the unknowns at the $p+1-$th iteration is evaluated solving the system of equation (37):

$$\left\{\begin{array}{c}d\mathbf{\Pi}\\ d\mathbf{\Gamma}\\ d\mathbf{\Lambda}\end{array}\right\} = -\left[\begin{array}{ccc}\dfrac{\partial \mathbf{R}_\pi}{\partial \mathbf{\Pi}} & \dfrac{\partial \mathbf{R}_\pi}{\partial \mathbf{\Gamma}} & \dfrac{\partial \mathbf{R}_\pi}{\partial \mathbf{\Lambda}}\\ \dfrac{\partial \mathbf{R}_\varepsilon}{\partial \mathbf{\Pi}} & \dfrac{\partial \mathbf{R}_\varepsilon}{\partial \mathbf{\Gamma}} & \dfrac{\partial \mathbf{R}_\varepsilon}{\partial \mathbf{\Lambda}}\\ \dfrac{\partial \mathbf{R}_g}{\partial \mathbf{\Pi}} & \dfrac{\partial \mathbf{R}_g}{\partial \mathbf{\Gamma}} & \dfrac{\partial \mathbf{R}_g}{\partial \mathbf{\Lambda}}\end{array}\right]_p^{-1} \left\{\begin{array}{c}\mathbf{R}_\pi\\ \mathbf{R}_\varepsilon\\ \mathbf{R}_g\end{array}\right\}_p. \tag{38}$$

At the end of the $p+1-$th iteration the residuals, given in equations (34), and the function g^s given in equations (35) should be reevaluated. In particular, the function f^s should be reevaluated with the internal value computed at the $p+1-$th iteration:

$$\begin{aligned}\overline{\boldsymbol{\varepsilon}}^s &= \overline{\mathbf{L}}^s_E\,\mathbf{E} + \overline{\mathbf{L}}^s_\Pi \mathbf{\Pi}\\ \boldsymbol{\sigma}^s &= \mathbf{C}^s\left(\overline{\boldsymbol{\varepsilon}}^s - \boldsymbol{\pi}^s\right)\\ q^s &= \sqrt{\frac{3}{2}\left(\boldsymbol{\sigma}^s\right)^T \mathbf{M}\,\boldsymbol{\sigma}^s},\\ f^s &= q^s - \sigma_y - H\kappa^s\end{aligned} \tag{39}$$

and then the function g^s, defined in equations (35), is determined as:

$$\begin{array}{rcll} g^s &=& \Delta\lambda^s & \text{if} \quad f^s < 0\\ g^s &=& q^s - \sigma_y - H\kappa^s & \text{if} \quad f^s \geq 0 \quad \text{Plasticity}\\ g^s &=& \triangle\lambda^s - \dfrac{1}{\mu}\left(\dfrac{q^s}{\sigma_y - H\kappa^s} - 1\right)^{1/\epsilon} & \text{if} \quad f^s \geq 0 \quad \text{Viscoplasticity}\end{array}. \tag{40}$$

The iterations will stop when the norm of the residual vector is lower than a prefixed tolerance.

4.2 Consistent tangent matrix

From formula (31), the overall stress is rewritten as:

$$\boldsymbol{\Sigma} = \overline{\mathbf{C}}\,\mathbf{E} + \sum_{j=1}^{n} \rho_j \left(\overline{\mathbf{L}}_E^j\right)^T \mathbf{C}^j \left(\overline{\mathbf{L}}_\Pi^j - \boldsymbol{\Delta}^j\right) (\Delta\boldsymbol{\Pi} + \boldsymbol{\Pi}_n)\,. \tag{41}$$

The overall tangent operator is obtained differentiating the overall stress given by formula (41) with respect to the overall strain:

$$\frac{\partial \boldsymbol{\Sigma}}{\partial \mathbf{E}} = \overline{\mathbf{C}} + \sum_{j=1}^{n} \rho_j \left(\overline{\mathbf{L}}_E^j\right)^T \mathbf{C}^j \left(\overline{\mathbf{L}}_\Pi^j - \boldsymbol{\Delta}^j\right) \frac{\partial \boldsymbol{\Pi}}{\partial \mathbf{E}}\,. \tag{42}$$

In order to evaluate the derivative $\partial\boldsymbol{\Pi}/\partial\mathbf{E}$, the vector $\boldsymbol{V} = \{\mathbf{R}_\pi\ \mathbf{R}_\varepsilon\ \mathbf{R}_g\}$ containing the residuals is introduced and its variation results:

$$d\mathbf{V}\left(\Delta\boldsymbol{\Pi}\,,\boldsymbol{,}\,\boldsymbol{\Gamma}\,,\boldsymbol{\Lambda}\,,\mathbf{E}\right) = \frac{\partial \mathbf{V}}{\partial \boldsymbol{\Pi}} d\boldsymbol{\Pi} + \frac{\partial \mathbf{V}}{\partial \boldsymbol{\Gamma}} d\boldsymbol{\Gamma} + \frac{\partial \mathbf{V}}{\partial \boldsymbol{\Lambda}} d\boldsymbol{\Lambda} + \frac{\partial \mathbf{V}}{\partial \mathbf{E}} d\mathbf{E} = \mathbf{0}\,, \tag{43}$$

which allows to obtain:

$$\left\{ \begin{array}{ccc} \dfrac{\partial \mathbf{V}}{\partial \boldsymbol{\Pi}} & \dfrac{\partial \mathbf{V}}{\partial \boldsymbol{\Gamma}} & \dfrac{\partial \mathbf{V}}{\partial \boldsymbol{\Lambda}} \end{array} \right\} \left\{ \begin{array}{c} \dfrac{d\boldsymbol{\Pi}}{d\mathbf{E}} \\ \dfrac{d\boldsymbol{\Gamma}}{d\mathbf{E}} \\ \dfrac{d\boldsymbol{\Lambda}}{d\mathbf{E}} \end{array} \right\} + \frac{\partial \mathbf{V}}{\partial \mathbf{E}} = \mathbf{0}\,. \tag{44}$$

Then, substituting $\boldsymbol{V} = \{\mathbf{R}_\pi\ \mathbf{R}_\varepsilon\ \mathbf{R}_g\}$ in equation (44) and solving, it results:

$$\left\{ \begin{array}{c} \dfrac{d\boldsymbol{\Pi}}{d\mathbf{E}} \\ \dfrac{d\boldsymbol{\Gamma}}{d\mathbf{E}} \\ \dfrac{d\boldsymbol{\Lambda}}{d\mathbf{E}} \end{array} \right\} = - \left[\begin{array}{ccc} \dfrac{\partial \mathbf{R}_\pi}{\partial \boldsymbol{\Pi}} & \dfrac{\partial \mathbf{R}_\pi}{\partial \boldsymbol{\Gamma}} & \dfrac{\partial \mathbf{R}_\pi}{\partial \boldsymbol{\Lambda}} \\ \dfrac{\partial \mathbf{R}_\varepsilon}{\partial \boldsymbol{\Pi}} & \dfrac{\partial \mathbf{R}_\varepsilon}{\partial \boldsymbol{\Gamma}} & \dfrac{\partial \mathbf{R}_\varepsilon}{\partial \boldsymbol{\Lambda}} \\ \dfrac{\partial \mathbf{R}_g}{\partial \boldsymbol{\Pi}} & \dfrac{\partial \mathbf{R}_g}{\partial \boldsymbol{\Gamma}} & \dfrac{\partial \mathbf{R}_g}{\partial \boldsymbol{\Lambda}} \end{array} \right]^{-1} \left\{ \begin{array}{c} \dfrac{\partial \mathbf{R}_\pi}{\partial \mathbf{E}} \\ \dfrac{\partial \mathbf{R}_\varepsilon}{\partial \mathbf{E}} \\ \dfrac{\partial \mathbf{R}_g}{\partial \mathbf{E}} \end{array} \right\}, \tag{45}$$

with

$$\begin{aligned} \frac{\partial \mathbf{R}_\pi}{\partial \mathbf{E}} &= \mathbf{0} \\ \frac{\partial \mathbf{R}_\varepsilon}{\partial \mathbf{E}} &= -\begin{bmatrix} \overline{\mathbf{L}}_E^1 \\ \overline{\mathbf{L}}_E^2 \\ .. \\ \overline{\mathbf{L}}_E^n \end{bmatrix} \\ \frac{\partial \mathbf{R}_g}{\partial \mathbf{E}} &= \mathbf{0} \end{aligned} \quad . \tag{46}$$

The first $6n$ rows of the vector computed from equation (45) give the derivative $\partial\mathbf{\Pi}/\partial\mathbf{E}$.

5 Numerical Applications

In the following, some numerical applications are presented concerning the multiscale analysis of structural elements made of composite materials. Two dimensional analyses are performed considering the plane stress condition. In particular, composite materials made of a periodic distribution of elastic inclusion in a plastic or viscoplastic matrix, are considered.

Two numerical applications are presented:

- multiscale analysis of a structure with a hole,
- comparison between multiscale and micromechanical structural analyses.

In both the multiscale analyses the ratio between the radius of the inclusion and the dimension of the structure is about 0.02, thus the assumption of scale separation can be considered fulfilled and the homogenization theory can be safely applied.

In developed the numerical applications, the UC is initially analyzed adopting the PWUTFA and the results of the homogenization procedure are compared with the ones recovered performing nonlinear micromechanical finite element analyses (FEM). Then, the analyses of the considered structural elements made of the composite material are developed adopting the multiscale approach, i.e. performing at each Gauss point the PWUTFA homogenization to determine the overall behavior of the composite material. For the finite element analyses the performing OPT three nodes triangular finite elements, proposed in [16] and recently modified in [5], are adopted. In particular, the multiscale scheme has been implemented in the MATLAB code developed in [5, 35].

5.1 Multiscale analysis of a structure with a hole

5.1.1 UC analysis

A UC, characterized by a circular inclusion with volume fraction equal to 25%, is studied. A local coordinate system (x_1, x_2) is introduced with the origin in the center of the UC. The UC has dimension $2a_1 \times 2a_2$. Because of the double symmetry, only half of the UC, represented in Figure 1, is studied prescribing the following boundary conditions:

$$\begin{array}{lcll} \mathbf{u}(-a_1,\ x_2) & = & \mathbf{u}(a_1,\ x_2) & 0 \leq x_2 \leq a_2 \\ \mathbf{u}(x_1,\ 0) & = & \mathbf{u}(x_1 + a_1,\ a_2) & -a_1 \leq x_1 \leq 0 \\ \mathbf{u}(x_1 + a_1,\ 0) & = & \mathbf{u}(x_1,\ a_2) & -a_1 \leq x_1 \leq 0 \end{array} \tag{47}$$

These boundary conditions applied to half of the UC allows to study all the loading conditions due to normal and shear strains recovering the same results that would be obtained studying the whole cell. The study of only a quarter of the UC with symmetric boundary conditions leads to correct results only when normal strain components are applied but not in the case of shear deformation. The nonlinear finite element micromechanical analysis is performed considering 2624 triangular elements with 4 Gauss points per element, so that the history variables is obtained as the product of the number of elements times the number of Gauss points times the number history variables for each Gauss point, resulting $2624 \times 4 \times 4 = 41984$.

For the PWUTFA approach, the UC is discretized in 27 subsets, reported in Figure 1. In particular, 26 subsets are adopted to model the plastic or viscoplastic matrix and in each subset the plastic strain is considered uniform, according to the PWUTFA technique described in the previous sections, and one elastic subset is used to model all the elastic inclusions, present in the studied UC. The number of history variables in each subset is equal to 4, i.e. 3 components of the inelastic strain and the accumulated inelastic strain; thus, for the half UC, the number of history variables for the homogenization analysis results to be $26 \times 4 = 104$. It can be remarked a drastic reduction of the number of history variables from the FEM approach to the PWUTFA technique, which is very important in the framework of the multiscale analysis.

The material properties adopted for the computations are reported in table 1. Four different composite materials are studied: three composites characterized by a viscoplastic matrix taking into account three different values of the non-dimensional rate sensitivity parameter $\epsilon = 0.1,\ 0.5,\ 1$; the fourth composite is made of a plastic matrix with the same yield stress and hardening parameter of the viscoplastic material.

Two different loading histories are studied. Firstly, the UC is considered subjected to a monotonic loading history in terms of the average strain E_{11}, until the value of 0.015 is

Constituent	E [GPa]	ν	σ_y [GPa]	h[GPa]	μ [s]	ϵ	dt [s]
Inclusion (elastic material)	400	0.2	-	-	-	-	-
Matrix (viscoplastic material)	180	0.3	0.075	0.416	500	0.1/0.5/1	0.01
Matrix (plastic material)	180	0.3	0.075	0.416	-	-	-

Table 1: Test 1 - Material properties of the constituents.

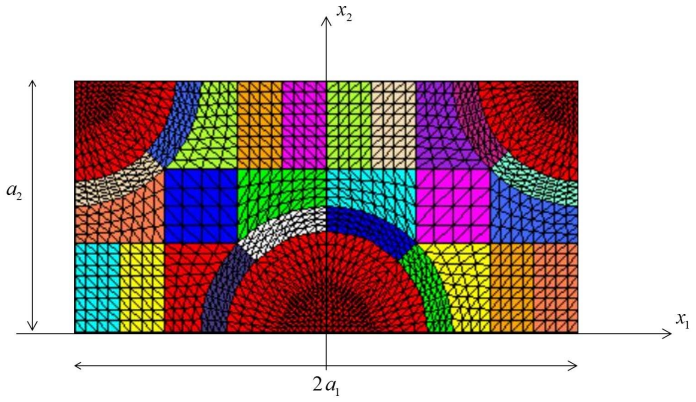

Figure 1: Division of the UC in 27 subsets.

reached. In Figures 2 and 3 the mechanical response of the UC in terms of Σ_{11} and Σ_{22} versus E_{11} is plotted for the PWUTFA homogenization and for the FEM analysis, respectively. It can be noted that the results of PWUTFA and FEM are in very good accordance for both the stresses and for all the composite materials studied so the proposed PWUTFA is able to describe the nonlinear response of the UC due to the plastic and viscoplastic effects occurring in the matrix.

Then, the UC is considered subjected to a monotonic loading history in terms of the average shear strain E_{12} until the value of 0.015 is reached.

In Figure 4, the shear response of the UC is reported plotting the overall stress Σ_{11} versus the average strain E_{11}. Also in this case the PWUTFA is able to describe the overall response of the cell, achieving results in good accordance with the FEM analysis. Decreasing the rate sensitivity parameter, the response of the UC becomes less ductile and it tends to a plateau achieved for a lower value of the load.

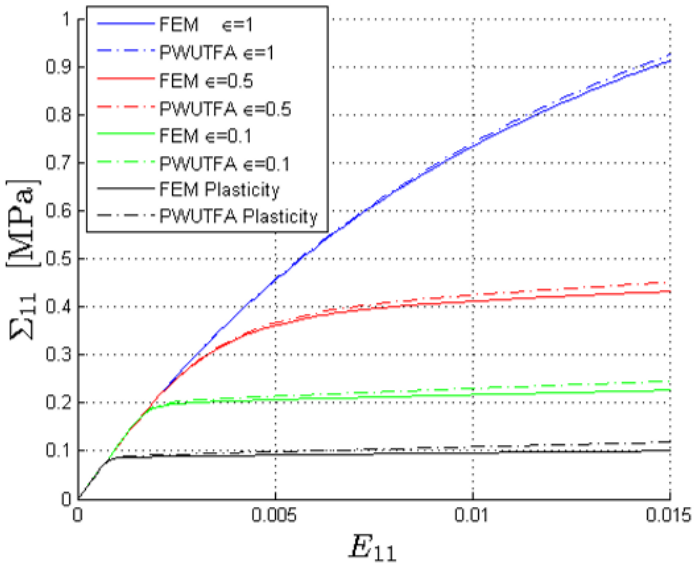

Figure 2: Mechanical response in terms of Σ_{11} versus E_{11}

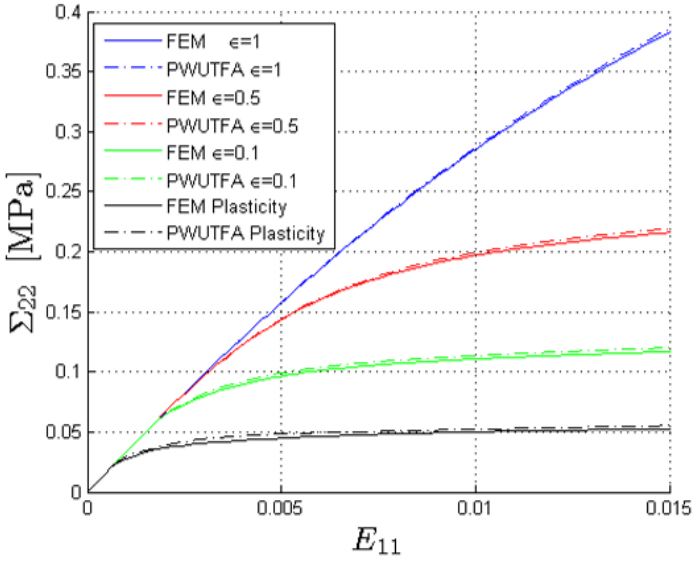

Figure 3: Mechanical response in terms of Σ_{22} versus E_{11}

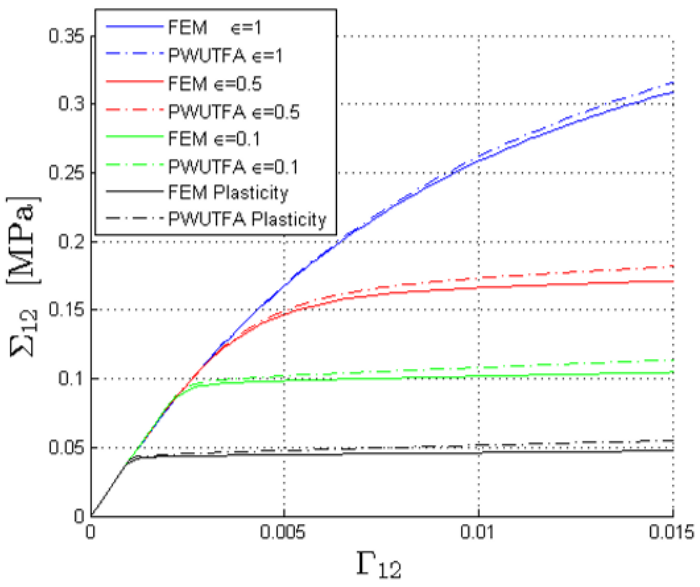

Figure 4: Mechanical response in terms of Σ_{12} versus E_{12}

5.1.2 Multiscale analysis

The structure, represented in Figure 5, made of the composite material with viscoplastic matrix and elastic inclusions, studied in the previous subsection with material properties reported in table 1, is analyzed. The structure is characterized by dimension L_1 =20 mm, L_2 =10 mm, thickness equal to 1 mm and by a hole with radius $R = 2$ mm. The double symmetry of the structure allows to study only a quarter of it, prescribing symmetry boundary conditions. The boundary and the loading conditions with the adopted discretization are represented in Figure 6. A displacement U along the X_1 direction is prescribed monotonically until the value 0.08 mm is reached while no body forces are applied. An unstructured mesh made of 548 three node triangular elements is adopted.

In Figure 7 the value of the resultant force F, obtained as of the sum of the reactions the constraints placed along the edge at $X_1 = 0$, versus the displacement U is plotted for the two different values of the parameter $\epsilon = 0.1$ and $\epsilon = 1$. It can be noted how the value of the parameter ϵ significantly influences the mechanical response of the structure. For a lower value of the non-dimensional rate sensitivity parameter, the response tends to have a lower maximum load and a lower ductility.

In Figure 8 the stress-strain response in terms of Σ_{11} versus E_{11} at the central Gauss point of three different finite elements, highlighted in the mesh represented in Figure 6, is plotted for the different values of ϵ. In Figures 9 the map distribution of three components of the average

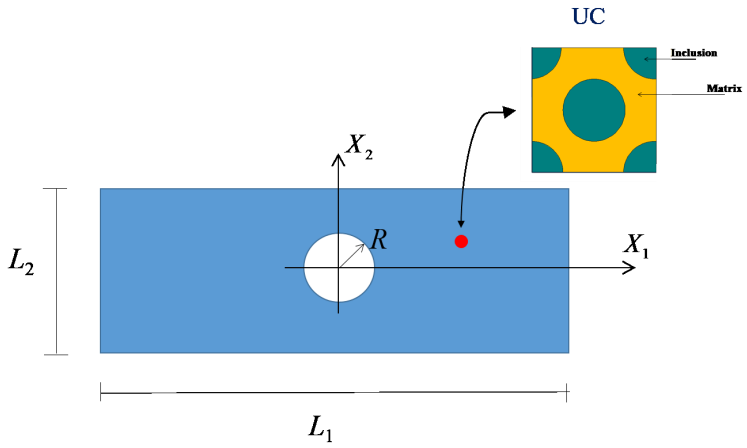

Figure 5: Geometry of the structure with a hole.

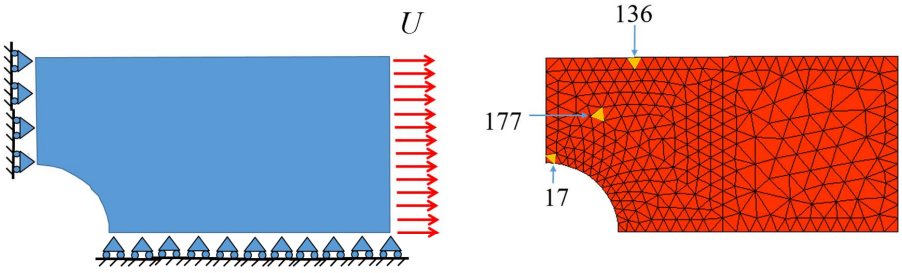

Figure 6: Adopted mesh, prescribed loading and boundary conditions.

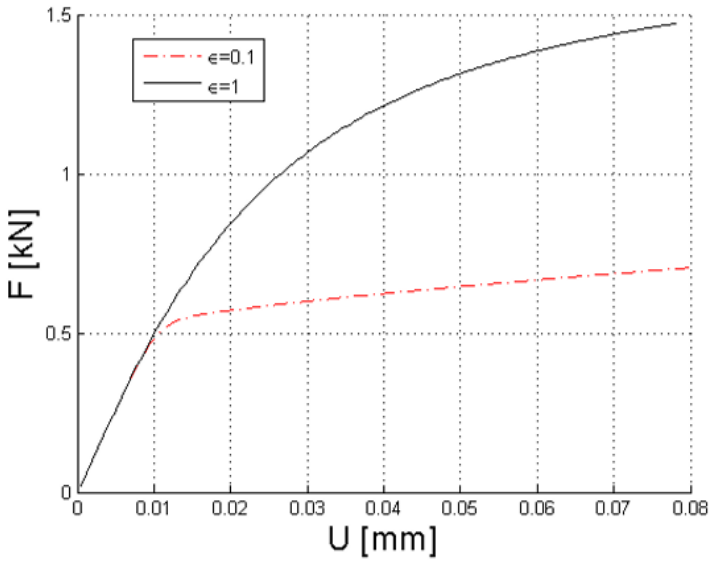

Figure 7: Mechanical response of the structure with the hole.

plastic strain $\overline{\mathbf{p}}$, given by equation (32), are plotted at the end of the analysis, respectively for $\epsilon = 0.1$ and $\epsilon = 1$. In these figures, it can be noted that plasticity effects occur in an area close to the hole and in a diagonal band starting from the hole, as expected. The highest value of the stress and of the strain is obtained in the finite element 17 close to the hole, while in the other two finite elements that belong to the diagonal band the values of stress and strain are of the same order of magnitude. In Figure 9 it can be noted that for $\epsilon = 1$ the plasticity effects are more significant and the area where they develop is larger than for $\epsilon = 0.1$. This effect can be noted also in Figure 8 where the stresses and the strains are higher in all the considered finite elements for the analysis with $\epsilon = 1$.

5.2 Comparison between multiscale and micromechanichal analysis

5.2.1 UC analysis

The same UC considered in the previous application, but characterized by the material properties of the constituents, reported in Table 2 is studied.

The analysis is developed considering the same discretization for the FEM analysis and the same subset distribution for the PWUTFA approach.

Two different loading histories are considered. First, the UC is considered subjected to a monotonic loading history in terms of horizontal average strain E_{11}, until the value of

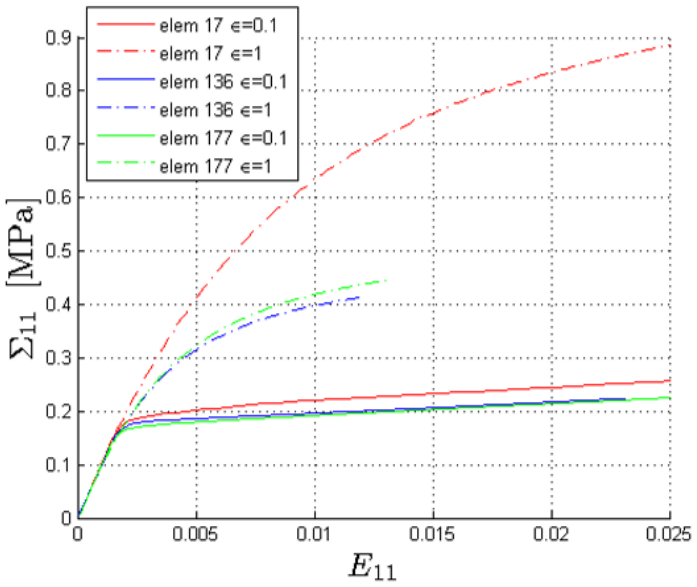

Figure 8: Stress and strain response of some finite elements of the structure.

Constituent	E [GPa]	ν	σ_y [GPa]	μ [s]	ϵ	h[GPa]
Inclusion (elastic material)	180	0.3	-	-	-	-
Matrix (viscoplastic material)	100	0.3	0.250	0.00025	1	10

Table 2: Test 2 - Material properties of the constituents.

0.015 is reached. In Figures 10 and 11 the mechanical response of the UC in terms of Σ_{11} and Σ_{22} versus E_{11} is plotted for the PWUTFA homogenization and for the FEM analysis, respectively. It can be noted that the results of PWUTFA and FEM are in very good accordance for both the stresses so the proposed PWUTFA is able to describe the nonlinear response of the UC due to the viscoplastic effects occurring in the matrix.

Then, the UC is considered subjected to a monotonic loading history in terms of the average shear strain E_{12} until the value of 0.015 is reached. In Figure 12 the mechanical response of the UC in terms of Σ_{12} versus E_{12} is plotted, comparing the PWUTFA homogenization and the FEM analysis results. Also in this case the PWUTFA is able to describe the overall response of the cell, achieving results in good accordance with the FEM analysis.

5.2.2 Multiscale analysis

The structure, represented in Figure 13, made of the composite material with a viscoplastic matrix and elastic inclusions, studied in the previous section, is analyzed. The structure is

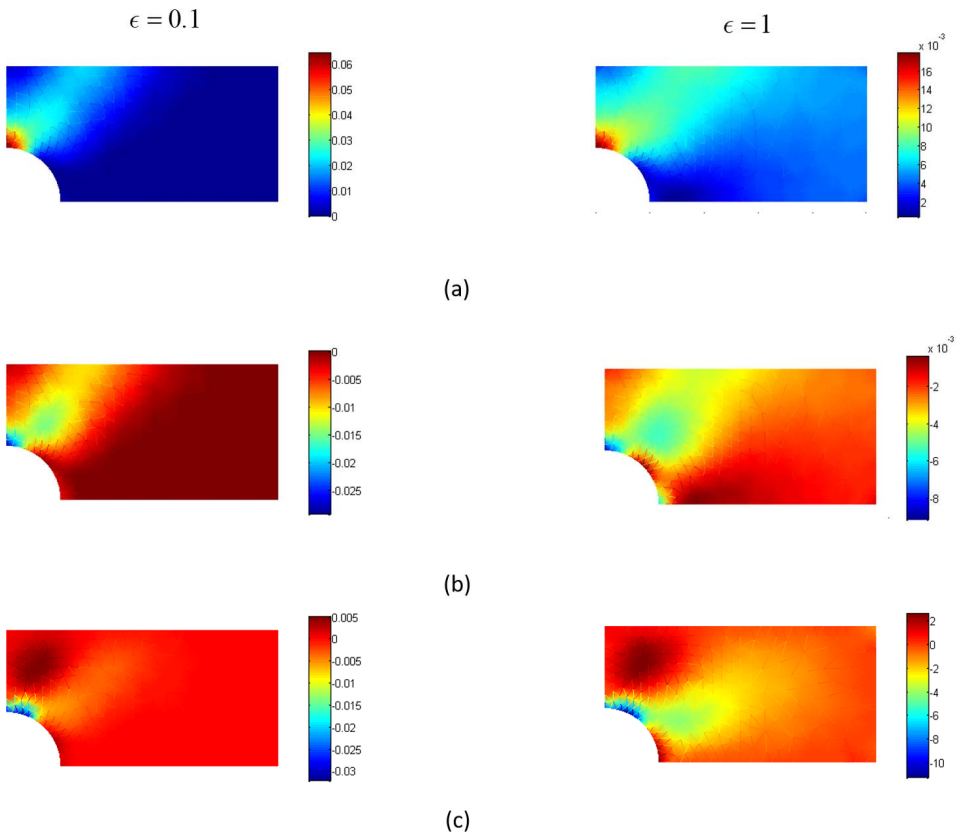

Figure 9: Distribution of the average plastic strain at the end of the analysis (a) axial in x_1 direction; (b) axial in x_2 direction; (c) shear.

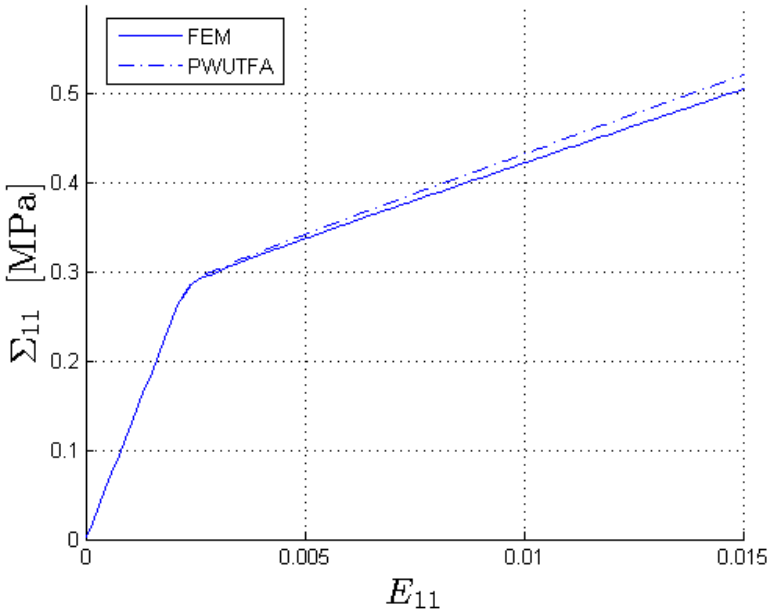

Figure 10: Mechanical response in terms of Σ_{11} versus E_{11}

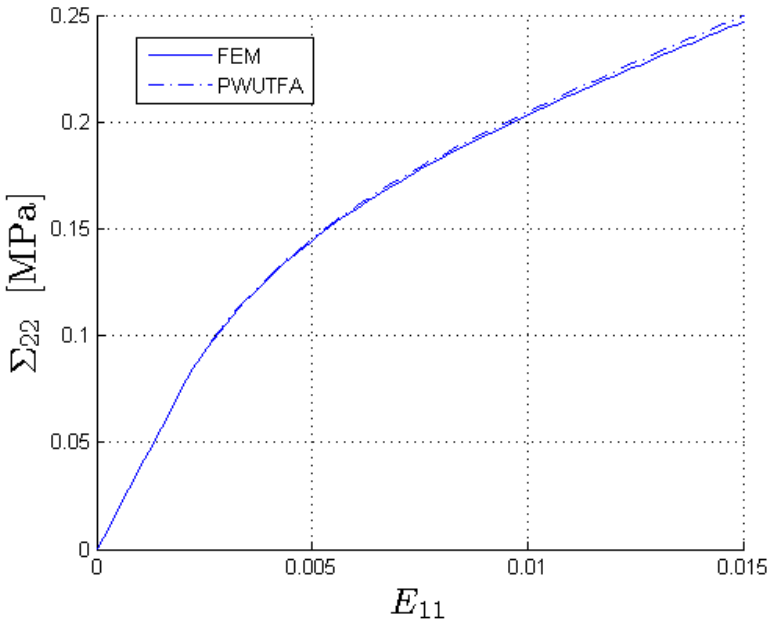

Figure 11: Mechanical response in terms of Σ_{22} versus E_{11}

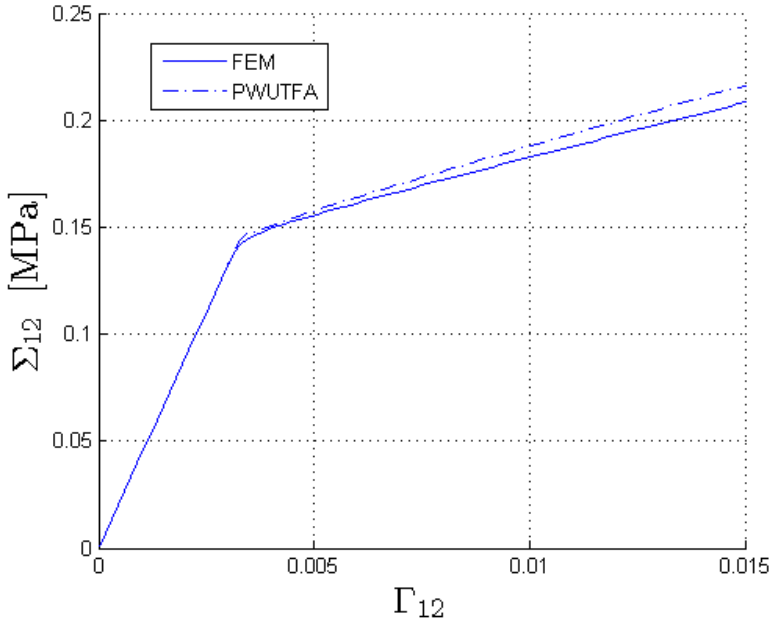

Figure 12: Mechanical response in terms of Σ_{12} versus E_{12}

characterized by the dimensions L_1 =10 mm, L_2 =20 mm and thickness equal to 1 mm. A coordinate system is introduced in Figure 13.

Two different approaches are developed.

- A multiscale analysis considering at each Gauss point of the triangular finite element the PWUTFA procedure, in order to derive the overall behavior of the composite material taking into account the nonlinear effects, is performed. For the multiscale analysis a mesh of 400 triangular element with 231 nodes is considered. At each Gauss point, the history variables of half of the UC should be stored, thus, the total number of history variables is $104 \times 4 \times 400 = 166400$.

- A micromechanical approach is also carried out. The discretization is obtained assembling ten UC in the horizontal direction and twenty UC in the vertical one. A mesh of 65600 triangular finite elements with 33221 nodes is adopted. Considering 4 history variables in each Gauss point, the total number of history variables results: $65600 \times 4 \times 4 = 1049600$.

It can be remarked that the multiscale approach reduces the number of history variables of one order of magnitude with respect to the micromechanical analysis. Moreover the number of equations depending of number of nodes, which defines the computation effort, is significantly lower in the multiscale approach.

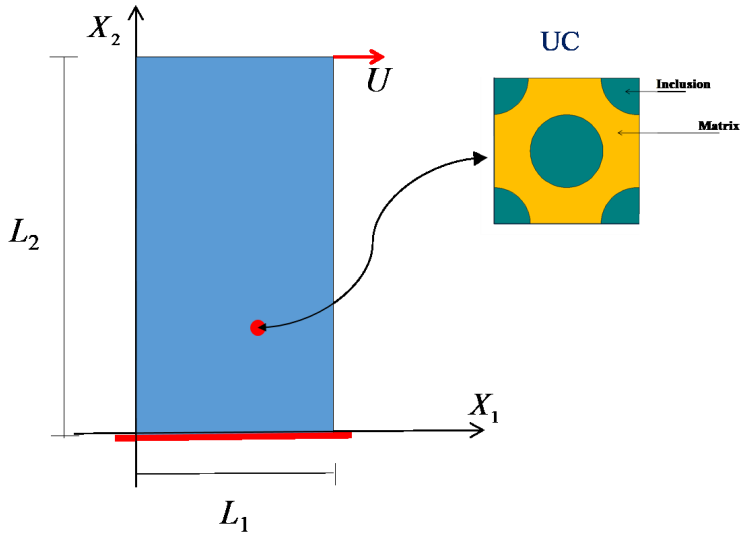

Figure 13: Geometry of the composite structure.

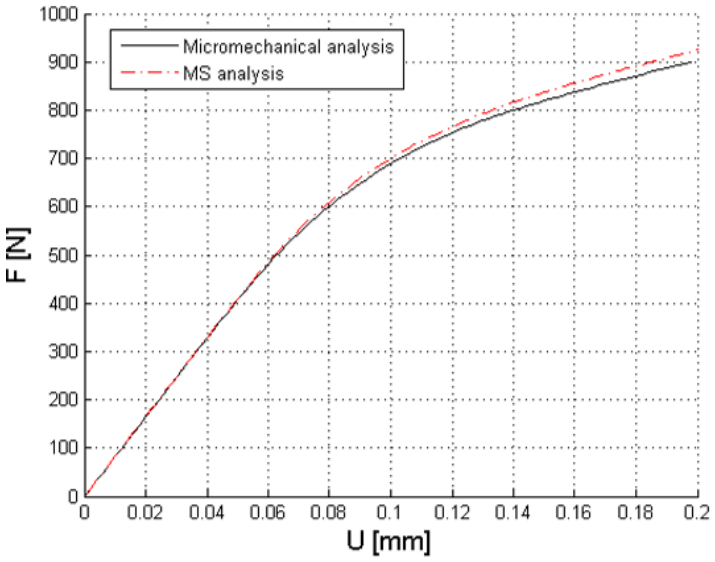

Figure 14: Mechanical response of the structure.

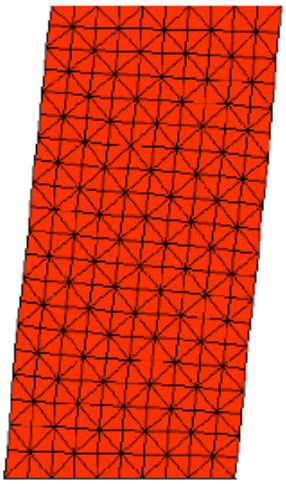

Figure 15: Deformation of the structure.

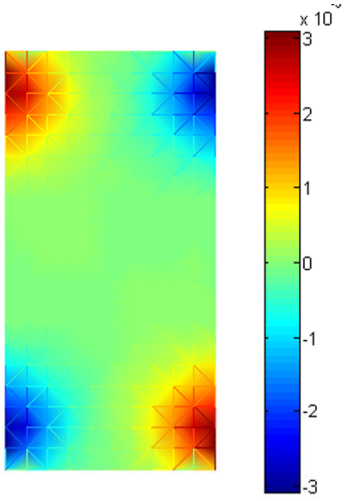

Figure 16: Distribution of the average plastic axial strain in X_1 direction at the end of the analysis.

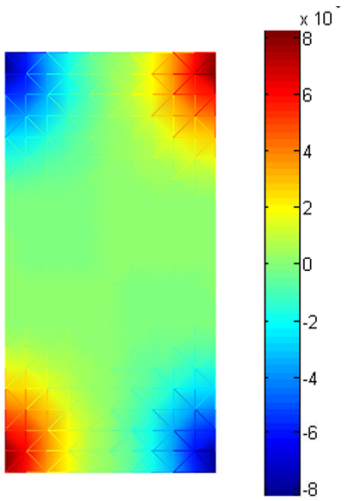

Figure 17: Distribution of the average plastic axial strain in X_2 direction at the end of the analysis.

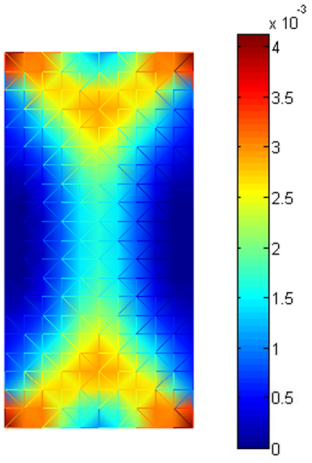

Figure 18: Distribution of the average plastic shear strain at the end of the analysis..

The structure is subjected to a loading history in terms of the displacement U prescribed in the X_1 direction at the nodes placed at the top of the structures. These nodes are constrained in the X_2 direction. The displacement U is increased until the value 0.2 mm is reached. In Figure 14 the mechanical response of the structure is plotted in terms of the total base reaction F versus the prescribed displacement U. In this figure the results of the multiscale (MS) analysis are compared with the micromechanical ones. It can be noted that there is a very good agreement during the whole loading history, thus the MS approach is able to lead to accurate results adopting a number of nodes, finite elements and history variables, significative reduced respect to the micromechanical analysis. In figure 15 the deformation configuration of the structure, obtained by the MS approach at the end of the loading history, is reported. In Figures 16, 17 and 18 the distribution of the average normal plastic strain in X_1 and X_2 direction and the average shear plastic strain are plotted at the end of the analysis, respectively.

It can be noted that the normal plasticity strains are concentrated in the corners of the structure and the shear plastic strain occurs mainly on the top and on the bottom of the structure.

6 Conclusions

An efficient multiscale procedure for studying the response of structural elements made of composite materials, whose constituents present plastic or viscoplastic response, is presented. The structural and the material scales are considered separated, thus a piecewise uniform TFA technique is proposed at the microlevel to model the behavior of periodic composites with a plastic or viscoplastic behavior of its constituents. The UC is divided in subsets and in each one the inelastic strain is considered uniform, i.e. constant. All the subset inelastic strains represent the history variables of the problem. A new efficient numerical procedure is proposed solving the evolutive problem in all the subsets, simultaneously. The tangent consistent with the algorithm is evaluated and adopted in the multiscale computations.

From the numerical applications, the PWUTFA procedure turns out to be able to give results in good accordance with the one obtained by a micromechanical nonlinear finite element analysis, considering a reasonable number of subsets and, consequently, drastically reducing the number of history variables. Composites with plastic and viscoplastic constituents, subjected to different loading history, are studied. All the presented applications confirm the efficiency of the proposed PWUTFA technique. Then, a structure with a hole is examined for different value of the non-dimensional rate sensitivity parameter. For higher value of ϵ

the area, where the inelastic strain occurs, becomes larger and higher values of the stress are reached close to the hole, as expected. The multiscale approach results to be a fundamental tool for designing the composite material as it allows to study the influence of each material properties of the constituents on the response of the structural element.

Furthermore, the response of a homogenized structure, obtained by the proposed multiscale approach, is compared with the response of the actual heterogeneous structure computed performing a micromechanical nonlinear structural finite element analysis with a very fine discretization. The results are in very good accordance. In fact, this comparison confirms the efficiency of the proposed multiscale approach that is able to reduced the history variables of one order of magnitude and the time of computation of one order of magnitude with respect to the nonlinear finite element structural micromechanical analysis.

The main innovation of the presented multiscale approach, with respect to the ones, already available in literature, is the efficiency of the numerical procedure developed to solve the micromechanical problem. In fact, it is based on an efficient modified Newton Raphson method and on the evaluation of the stiffness tangent consistent with the algorithm that contribute significantly to reduce the computational burden of the multiscale analysis.

Finally, the presented multiscale procedure can be extended to the study of composite materials characterized by other nonlinear behavior, as for instance shape memory effect, and also damage and fracture.

Acknowledgments

Financial support by the Italian Ministry of Education, University and Research - MIUR, project PRIN2015 Multi-scale mechanical models for the design and optimization of micro-structured smart materials and metamaterials (prot. 2015LYYXA8_002, CUP H32F15000090005), is gratefully acknowledged.

The authors would like to thank Prof. Paolo Bisegna for his useful suggestions for the implementation of the extension of his FE code to the multiscale analysis.

References

[1] M. Agoras, R. Avazmohammadi, and P. Ponte-Castañeda. Incremental variational procedure for elasto-viscoplastic composites and application to polymer- and metal-matrix composites reinforced by spheroidal elastic particles. *International Journal of Solids and Structures*, 2016.

[2] R.M. Bajracharya, A.C. Manalo, W. Karunasena, and K.-T. Lau. Durability characteristics and property prediction of glass fibre reinforced mixed plastics composites. *Composites Part B: Engineering*, 116:16 – 29, 2017.

[3] A. Caporale, L. Feo, and R. Luciano. Eigenstrain and Fourier series for evaluation of elastic local fields and effective properties of periodic composites. *Composites Part B: Engineering*, 81:251 – 258, 2015.

[4] A. Caporale, R. Luciano, and R. Penna. Fourier series expansion in non-orthogonal coordinate system for the homogenization of linear viscoelastic periodic composites. *Composites Part B: Engineering*, 54:241 – 245, 2013.

[5] F. Caselli and P. Bisegna. Polar decomposition based corotational framework for triangular shell elements with distributed loads. *International Journal for Numerical Methods in Engineering*, 95(6):499–528, 2013.

[6] J. Chaboche, L.S. Kruch, J. Maire, and T. Pottier. Towards a micromechanics based inelastic and damage modeling of composites. *International Journal of Plasticity*, 17:411–439, 2001.

[7] Q. Chen, X. Chen, Z. Zhai, and Z. Yang. A new and general formulation of three-dimensional finite-volume micromechanics for particulate reinforced composites with viscoplastic phases. *Composites Part B: Engineering*, 85:216 – 232, 2016.

[8] G. Colonnetti. Su certi stati di coazione elastica che non dipendono da azioni esterne. *Rendiconti della R. Accademia dei Lincei*, giugno:43–47, 1917.

[9] F. Covezzi, S. de Miranda, S. Marfia, and E. Sacco. Complementary formulation of the TFA for the elasto-plastic analysis of composites. *Composite Structures*, 2016.

[10] F. Covezzi, S. de Miranda, S. Marfia, and E. Sacco. Homogenization of elastic-viscoplastic composites by the mixed TFA. *Comput Methods Appl Mech Eng*, 318:701–723, 2017.

[11] C. Czarnota, K. Kowalczyk-Gajewska, A. Salahouelhadj, M. Martiny, and S. Mercier. Modeling of the cyclic behavior of elastic-viscoplastic composites by the additive tangent Mori-Tanaka approach and validation by finite element calculations. *International Journal of Solids and Structures*, 56-57:96 – 117, 2015.

[12] E.A. de Souza Neto, D. Perić, and D.R.J. Owen. *Computational Methods For Plasticity: Theory and Applications*. Wiley, 2008.

[13] A. Dean, S. Sahraee, J. Reinoso, and R. Rolfes. A new invariant-based thermo-plastic model for finite deformation analysis of short fibre reinforced composites: Development and numerical aspects. *Composites Part B: Engineering*, In press, 2017.

[14] G.J. Dvorak. Transformation field analysis of inelastic composite materials. *Proceedings of the Royal Society of London A*, 437:311–327, 1992.

[15] G.J. Dvorak and A. Bahei-El-Din. Inelastic composite materials: transformation field analysis and experiments. *In: Suquet, P. (Ed.), Continuum Micromechanics, CISM Course and Lecture*, 377:1–59, 1997.

[16] C.A. Felippa. A study of optimal membrane triangles with drilling freedoms. *Comput Methods Appl Mech Eng*, 192(16-18):2125–2168, 2003.

[17] F. Feyel and J.L. Chaboche. FE^2 multiscale approach for modelling the elastoviscoplastic behaviour of long fiber SiC/Ti composite materials. *Comput. Methods Appl. Mech. Eng.*, 183:309–330, 2000.

[18] P. Franciosi and S. Berbenni. Heterogeneous crystal and poly-crystal plasticity modeling from transformation field analysis within a regularized Schimd law. *Journal of Mechanics and Physics of Solids*, 55:2265–2299, 2007.

[19] P. Franciosi and S. Berbenni. Multi-laminate plastic-strain organization for nonuniform tfa modeling of poly-crystal regularized plastic flow. *International Journal of Plasticity*, 24:1549–1580, 2008.

[20] F. Fritzen and T. Böhlke. Nonuniform transformation field analysis of materials with morphological anisotropy. *Composites Science and Technology*, 71:433–442, 2011.

[21] F. Fritzen and M Hodapp. The finite element square reduced (FE 2R) method with GPU acceleration: towards three-dimensional two-scale simulations. *Int. J. Numer. Methods Eng.*, 107(10):853–881, 2016.

[22] F. Fritzen, M. Hodapp, and M. Leuschner. GPU accelerated computational homogenization based on a variational approach in a reduced basis framework. *Computer Methods in Applied Mechanics and Engineering*, 278:186–217, 2014.

[23] F. Fritzen and M. Leuschner. Reduced basis hybrid computational homogenization based on a mixed incremental formulation. *Computer Methods in Applied Mechanics and Engineering*, 260:143–154, 2013.

[24] F. Fritzen and M. Leuschner. Reduced order homogenization for viscoplastic composite materials including dissipative imperfect interfaces. *Mechanics of Materials*, 104:121–238, 2017.

[25] F. Fritzen, S. Marfia, and V. Sepe. Reduced order modeling in nonlinear homogenization: A comparative study. *Computers and Structures*, 157:114–131, 2015.

[26] P. Gudlur, A. Muliana, and M. Radovic. Effective thermo-mechanical properties of aluminum-alumina composites using numerical approach. *Composites Part B: Engineering*, 58:534 – 543, 2014.

[27] B. Koohestani, I. Ganetri, and E. Yilmaz. Effects of silane modified minerals on mechanical, microstructural, thermal, and rheological properties of wood plastic composites. *Composites Part B: Engineering*, 111:103 – 111, 2017.

[28] C. Mareau and S. Berbenni. An affine formulation for the self-consistent modeling of elasto-viscoplastic heterogeneous materials based on the translated field method. *International Journal of Plasticity*, 64:134 – 150, 2015.

[29] S. Marfia. Micro-macro analysis of shape memory alloy composites. *Int. J. of Solids Struct.*, 42:3677–3699, 2005.

[30] S. Marfia and E. Sacco. Micromechanics and homogenization of SMA-wire-reinforced materials. *Journal of Applied Mechanics*, 72:259–268, 2005.

[31] S. Marfia and E. Sacco. Analysis of SMA composite laminates using a multiscale modeling technique. *Int. J. Numer. Meth. Eng.*, 70:1182–1208, 2007.

[32] S. Marfia and E. Sacco. Computational homogenization of composites experiencing plasticity, cracking and debonding phenomena. *Computer Methods in Applied Mechanics and Engineering*, 304:319 – 341, 2016.

[33] J.C. Michel and P. Suquet. Nonuniform transformation field analysis. *International Journal of Solids and Structures*, 40:6937–6955, 2003.

[34] J.C. Michel and P. Suquet. Computational analysis of nonlinear composite structures using the nonuniform transformation field analysis. *Computer Methods in Applied Mechanics and Engineering*, 193:5477–5502, 2004.

[35] N. Nodargi and P. Bisegna. A novel high-performance mixed membrane finite element for the analysis of inelastic structures. *Computers and Structures*, 182:337–353, 2017.

[36] P. Perzyna. Fundamental problems in viscoplasticity. *Advances in Applied Mechanics*, 9(1):243 – 377, 1968.

[37] P. Ponte-Castañeda. New variational principles in plasticity and their application to composite materials. *Journal of the Mechanics and Physics of Solids*, 40(8):1757 – 1788, 1992.

[38] S. Roussette, J.C. Michel, and P. Suquet. Nonuniform transformation field analysis of elastic-viscoplastic composites. *Composites Science and Technology*, 69:22–27, 2009.

[39] T. Sabiston, M. Mohammadi, M. Cherkaoui, J. Lévesque, and Kaan Inal. Micromechanics based elasto-visco-plastic response of long fibre composites using functionally graded interphases at quasi-static and moderate strain rates. *Composites Part B: Engineering*, 100:31 – 43, 2016.

[40] E. Sacco. A nonlinear homogenization procedure for periodic masonry. *European Journal of Mechanics, A/Solids*, 28:209–222, 2009.

[41] V. Sepe, S. Marfia, and E. Sacco. A nonuniform TFA homogenization technique based on piecewise interpolation functions of the inelastic field. *International Journal of Solids and Structures*, 50:725–742, 2013.

[42] A. Alipour Skandani and M. Al-Haik. Viscoplastic characterization and modeling of hybrid carbon fiber/carbon nanotubes reinforced composites. *Composites Part B: Engineering*, 99:63 – 74, 2016.

[43] S. Zhang and C. Oskay. Reduced order variational multiscale enrichment method for elasto-viscoplastic problems. *Comput. Methods Appl. Mech. Engrg.*, 300:199–224, 2016.

Appendix

In the following the derivatives appearing in equation (38) are calculated:

$$\frac{\partial \mathbf{R}_\pi}{\partial \mathbf{\Pi}} = \mathbf{I} - \frac{\partial}{\partial \mathbf{\Pi}} \left\{ \begin{array}{c} \Delta\lambda^1 \frac{\partial f^1}{\partial \boldsymbol{\sigma}^1} \\ \Delta\lambda^2 \frac{\partial f^2}{\partial \boldsymbol{\sigma}^2} \\ \ldots \\ \Delta\lambda^n \frac{\partial f^n}{\partial \boldsymbol{\sigma}^n} \end{array} \right\} = \mathbf{I} - \left[\begin{array}{cccc} \Delta\lambda^1 \frac{\partial^2 f^1}{\partial \boldsymbol{\pi}^1 \partial \boldsymbol{\sigma}^1} & \mathbf{0} & \ldots & \mathbf{0} \\ \mathbf{0} & \Delta\lambda^2 \frac{\partial^2 f^2}{\partial \boldsymbol{\pi}^2 \partial \boldsymbol{\sigma}^2} & \ldots & \mathbf{0} \\ \ldots & \ldots & \ldots & \ldots \\ \mathbf{0} & \mathbf{0} & \ldots & \Delta\lambda^n \frac{\partial^2 f^n}{\partial \boldsymbol{\pi}^n \partial \boldsymbol{\sigma}^n} \end{array} \right]$$

$$\frac{\partial \mathbf{R}_\pi}{\partial \mathbf{\Gamma}} = -\frac{\partial}{\partial \mathbf{\Gamma}} \left\{ \begin{array}{c} \Delta\lambda^1 \frac{\partial f^1}{\partial \boldsymbol{\sigma}^1} \\ \Delta\lambda^2 \frac{\partial f^2}{\partial \boldsymbol{\sigma}^2} \\ \ldots \\ \Delta\lambda^n \frac{\partial f^n}{\partial \boldsymbol{\sigma}^n} \end{array} \right\} = - \left[\begin{array}{cccc} \Delta\lambda^1 \frac{\partial^2 f^1}{\partial \overline{\boldsymbol{\varepsilon}}^1 \partial \boldsymbol{\sigma}^1} & \mathbf{0} & \ldots & \mathbf{0} \\ \mathbf{0} & \Delta\lambda^2 \frac{\partial^2 f^2}{\partial \overline{\boldsymbol{\varepsilon}}^2 \partial \boldsymbol{\sigma}^2} & \ldots & \mathbf{0} \\ \ldots & \ldots & \ldots & \ldots \\ \mathbf{0} & \mathbf{0} & \ldots & \Delta\lambda^n \frac{\partial^2 f^n}{\partial \overline{\boldsymbol{\varepsilon}}^n \partial \boldsymbol{\sigma}^n} \end{array} \right]$$

$$\frac{\partial \mathbf{R}_\pi}{\partial \mathbf{\Lambda}} = -\frac{\partial}{\partial \mathbf{\Lambda}} \left\{ \begin{array}{c} \Delta\lambda^1 \frac{\partial f^1}{\partial \boldsymbol{\sigma}^1} \\ \Delta\lambda^2 \frac{\partial f^2}{\partial \boldsymbol{\sigma}^2} \\ \ldots \\ \Delta\lambda^n \frac{\partial f^n}{\partial \boldsymbol{\sigma}^n} \end{array} \right\} = - \left[\begin{array}{cccc} \frac{\partial f^1}{\partial \boldsymbol{\sigma}^1} & \mathbf{0} & \ldots & \mathbf{0} \\ \mathbf{0} & \frac{\partial f^2}{\partial \boldsymbol{\sigma}^2} & \ldots & \mathbf{0} \\ \ldots & \ldots & \ldots & \ldots \\ \mathbf{0} & \mathbf{0} & \ldots & \frac{\partial f^n}{\partial \boldsymbol{\sigma}^n} \end{array} \right]$$

$$\frac{\partial \mathbf{R}_\varepsilon}{\partial \mathbf{\Pi}} = - \left[\begin{array}{c} \overline{\mathbf{R}}^1_{\mathbf{\Pi}} \\ \overline{\mathbf{R}}^2_{\mathbf{\Pi}} \\ \ldots \\ \overline{\mathbf{R}}^n_{\mathbf{\Pi}} \end{array} \right]$$

$$\frac{\partial \mathbf{R}_\varepsilon}{\partial \mathbf{\Gamma}} = \mathbf{I}$$

$$\frac{\partial \mathbf{R}_\varepsilon}{\partial \mathbf{\Lambda}} = \mathbf{0}$$

$$\frac{\partial \mathbf{R}_g}{\partial \mathbf{\Pi}} = \left[\begin{array}{cccc} \frac{\partial g^1}{\partial \boldsymbol{\pi}^1} & \mathbf{0} & \ldots & \mathbf{0} \\ \mathbf{0} & \frac{\partial g^2}{\partial \boldsymbol{\pi}^2} & \ldots & \mathbf{0} \\ \ldots & \ldots & \ldots & \ldots \\ \mathbf{0} & \mathbf{0} & \ldots & \frac{\partial g^n}{\partial \boldsymbol{\pi}^n} \end{array} \right]$$

$$\frac{\partial \mathbf{R}_g}{\partial \mathbf{\Gamma}} = \left[\begin{array}{cccc} \frac{\partial g^1}{\partial \overline{\boldsymbol{\varepsilon}}^1} & \mathbf{0} & \ldots & \mathbf{0} \\ \mathbf{0} & \frac{\partial g^2}{\partial \overline{\boldsymbol{\varepsilon}}^2} & \ldots & \mathbf{0} \\ \ldots & \ldots & \ldots & \ldots \\ \mathbf{0} & \mathbf{0} & \ldots & \frac{\partial g^n}{\partial} \end{array} \right]$$

$$\frac{\partial \mathbf{R}_g}{\partial \mathbf{\Lambda}} = \left[\begin{array}{cccc} \frac{\partial g^1}{\partial \lambda^1} & \mathbf{0} & \ldots & \mathbf{0} \\ \mathbf{0} & \frac{\partial g^2}{\partial \lambda^2} & \ldots & \mathbf{0} \\ \ldots & \ldots & \ldots & \ldots \\ \mathbf{0} & \mathbf{0} & \ldots & \frac{\partial g^n}{\partial \lambda^n} \end{array} \right]$$

In the above formulas, the derivatives in the subset s (with $s = 1..n$) result:

$$\frac{\partial^2 f^s}{\partial \boldsymbol{\pi}^s \partial \boldsymbol{\sigma}^s} = -\frac{\partial^2 f^s}{\partial \boldsymbol{\sigma}^2}\mathbf{C}^s$$

$$\frac{\partial^2 f^s}{\partial \overline{\boldsymbol{\varepsilon}}^s \partial \boldsymbol{\sigma}^s} = \frac{\partial^2 f^s}{\partial \left(\boldsymbol{\sigma}^s\right)^2}\mathbf{C}^s$$

$$\frac{\partial g^s}{\partial \boldsymbol{\pi}^s} = \begin{cases} 0 & \text{if} \quad f^{s,TR} < 0 \\ -\mathbf{C}^s\,\mathbf{N}^s & \text{if} \quad f^{s,TR} \geq 0 \qquad \text{Plasticity} \\ \frac{\mathbf{C}^s\,\mathbf{N}^s dt}{\mu\epsilon(\sigma_y - H\kappa^s)}\left(\frac{q^s}{\sigma_y - H\kappa^s} - 1\right)^{\frac{1}{\epsilon}-1} & \text{if} \quad f^{s,TR} \geq 0 \qquad \text{Viscoplasticity} \end{cases}$$

$$\frac{\partial g^s}{\partial \overline{\boldsymbol{\varepsilon}}^s} = \begin{cases} 0 & \text{if} \quad f^{s,TR} < 0 \\ \mathbf{C}^s\,\mathbf{N}^s & \text{if} \quad f^{s,TR} \geq 0 \qquad \text{Plasticity} \\ -\frac{\mathbf{C}^s\,\mathbf{N}^s dt}{\mu\epsilon(\sigma_y - H\kappa^s)}\left(\frac{q^s}{\sigma_y - H\kappa^s} - 1\right)^{\frac{1}{\epsilon}-1} & \text{if} \quad f^{s,TR} \geq 0 \qquad \text{Viscoplasticity} \end{cases}$$

$$\frac{\partial g^s}{\partial \lambda^s} = \begin{cases} 1 & \text{if} \quad f^{s,TR} < 0 \\ -H & \text{if} \quad f^{s,TR} \geq 0 \qquad \text{Plasticity} \\ 1 + \frac{q^s\,H\,dt}{\mu\epsilon(\sigma_y - H\kappa^s)^2}\left(\frac{q^s}{\sigma_y - H\kappa^s} - 1\right)^{\frac{1}{\epsilon}-1} & \text{if} \quad f^{s,TR} \geq 0 \qquad \text{Viscoplasticity} \end{cases}$$

with

$$\frac{\partial^2 f^s}{\partial \left(\boldsymbol{\sigma}^s\right)^2} = \frac{3}{2\,q^s}\left[\mathbf{M} - \frac{3}{2\,\left(q^s\right)^2}\mathbf{M}\boldsymbol{\sigma}^s\left(\mathbf{M}\,\boldsymbol{\sigma}^s\right)\right]$$